Supplementary Information (SI) for Nanoscale.

Supporting Information

Design and Synthesis of Hydrogenated Carbon Nanomaterials for Perovskite Solar Cells

Sanan Appapillai,[‡a] Sharmin Akter,[‡b] Tajamul Syed,[c] Hui Wang,*[b,d] and Wei Wei*[a]

[a]*Department of Mechanical and Aerospace Engineering, Michigan Technological University, 1400 Townsend Dr., Houghton, MI 49931, USA.*

[b]*Department of Mechanical Engineering, University of Louisville, 2301 South 3rd St., Louisville, KY 40292, USA.*

[c]*Department of Mechanical Engineering, Wichita State University, 1845 Fairmount St., Wichita, KS 67260, USA.*

[d]*Conn Center for Renewable Energy, University of Louisville, 2301 South 3rd St., Louisville, KY 40292, USA.*

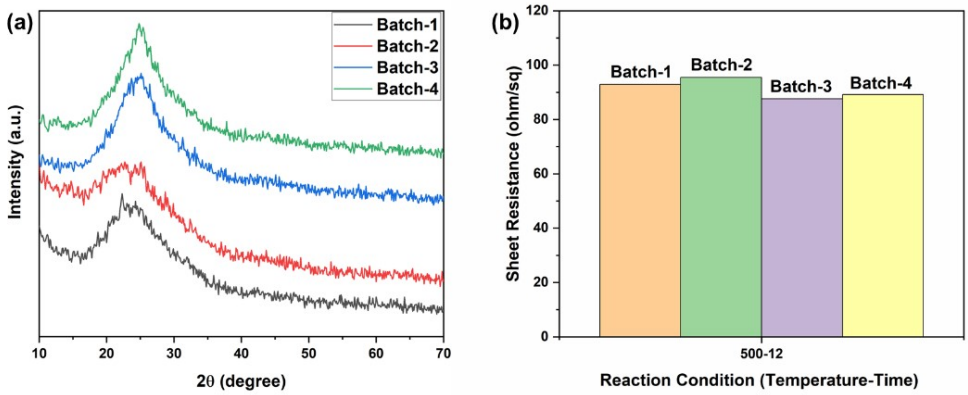

Figure S1. (a) XRD spectrum and (b) sheet resistance of carbon nanosheets from four different batches.

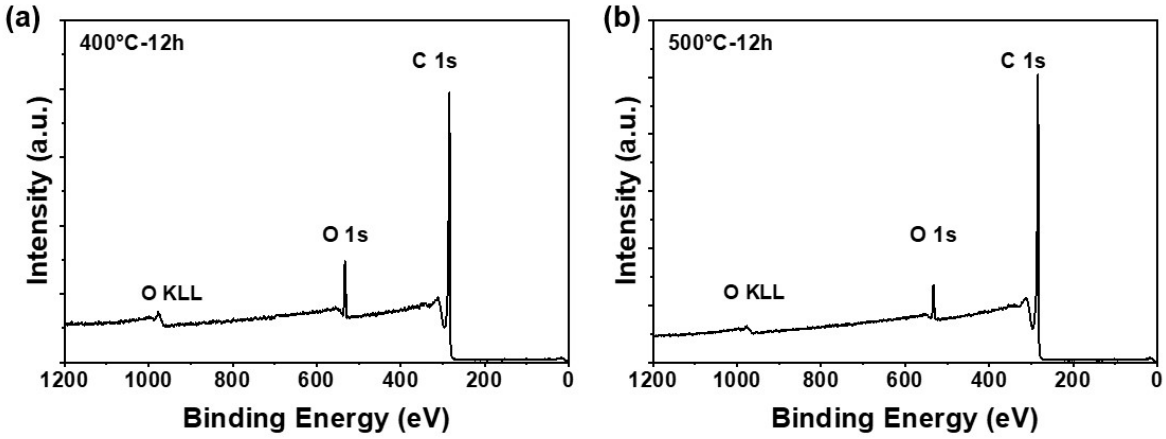

Figure S2. XPS spectra of synthesized carbon after heating treatment at (a) 400° C for 12 h and (b) 500° C for 12 h.

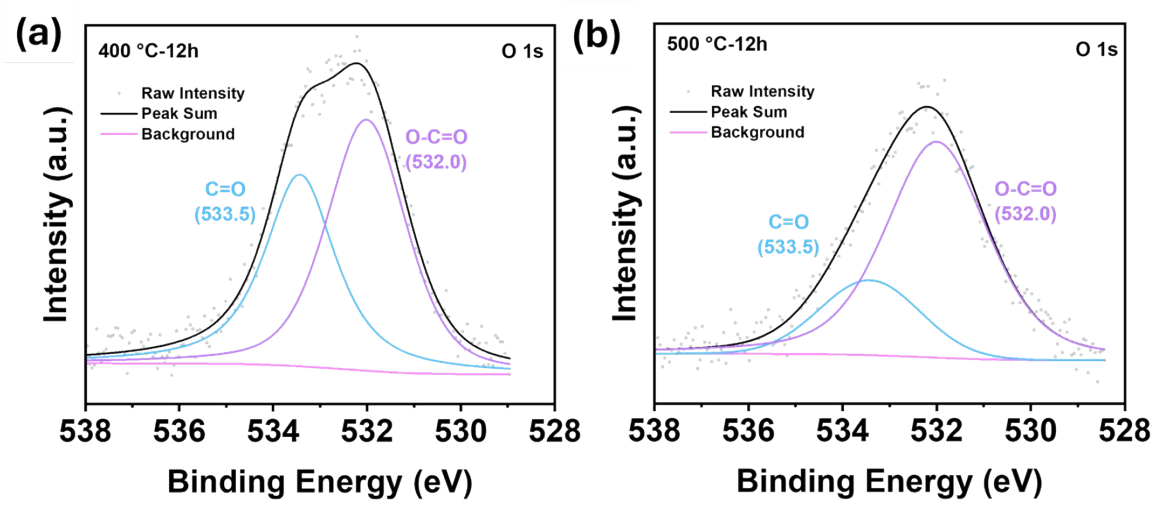

Figure S3. XPS O1s spectra of synthesized carbon after heating treatment at (a) 400° C for 12 h and (b) 500° C for 12 h.

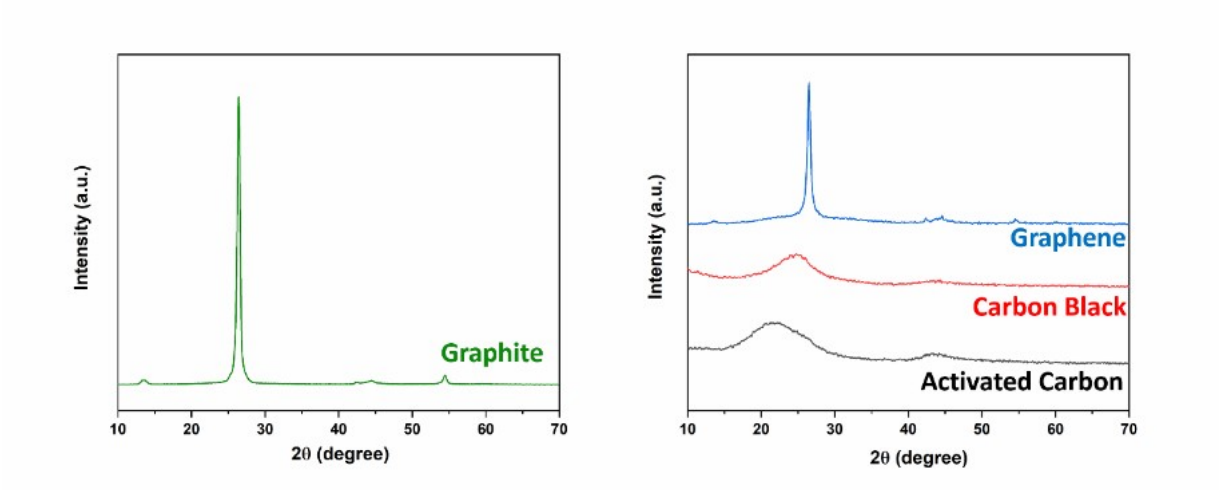

Figure S4. XRD patterns of commercial carbon materials (activated carbon, carbon black, graphite, and graphene).

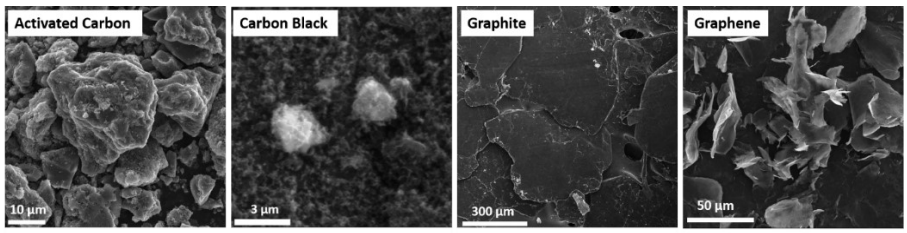

Figure S5. SEM images of commercial carbon materials: activated carbon, carbon black, graphite, and graphene.

Table S1. Elemental Analysis of commercial carbon materials.

Samples	Carbon (%)	Hydrogen (%)	Oxygen (%)	Nitrogen (%)
Activated Carbon	68.75	0.39	25.65	5.21
Carbon Black	96.30	0.33	1.28	0.11
Graphite	98.25	-	1.75	-
Graphene	96.64	0.25	3.11	-

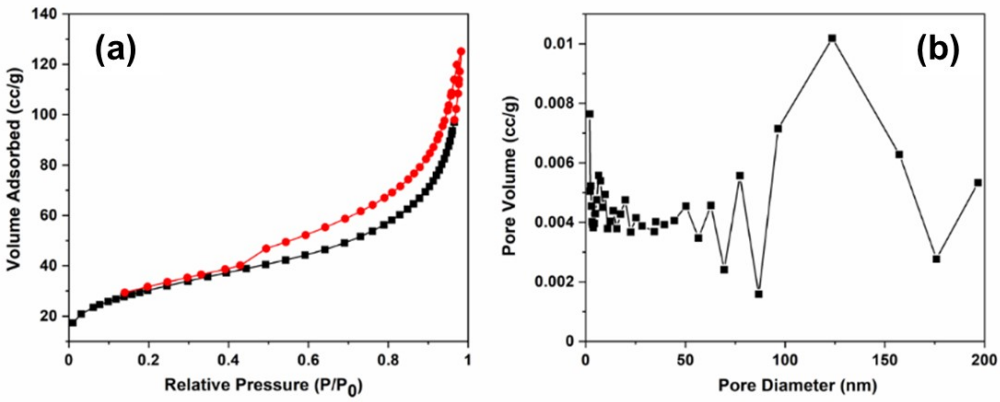

Figure S6. (A) The N_2 adsorption–desorption isothermals for carbon black. (B) Pore size distribution of carbon black.

Figure S6A shows that the N_2 adsorption-desorption isotherm of carbon black is type II according to the IPUAC classification having H3 type hysteresis loop. Moreover, from Figure S6B, the pore size distribution is mainly concentrated between 100-150 nm. The BET surface area was measured to be 109 m^2/g.

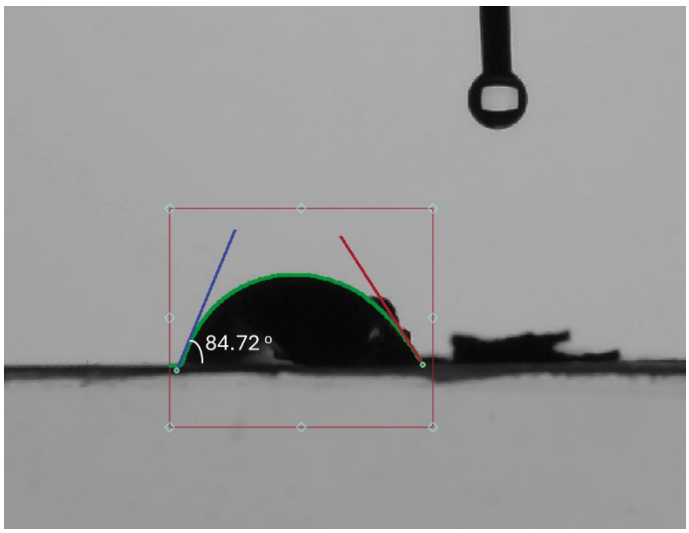

Figure S7. The contact angle of carbon black film.

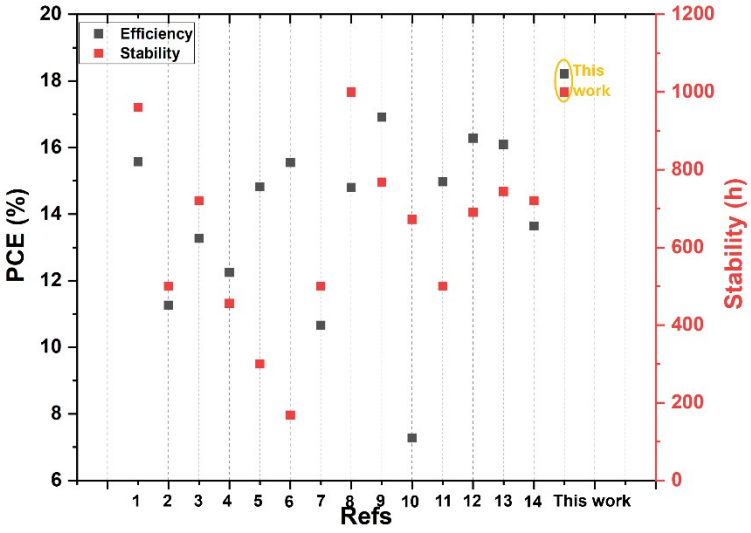

Figure S8. Comparison of efficiency and stability between the present work and reported literature.[S1-S14]

References:

(S1) Zhang, M.; Li, W.; Zhao, W.; Han, X. Enhancing Charge Carrier Transport in the Carbon-Electrode-Based CsPbI2Br Perovskite Solar Cells via I/Br Homogenization Process Modulation and Oleic Acid Surface Passivation. *ACS Applied Energy Materials* **2023**, *6* (5), 2973–2980.
(S2) Shi, Z.; Li, S.; Min, C.; Xie, J.; Ma, R. Modification of energy levels by cetyltrimethylammonium bromide at the perovskite/carbon interface for highly efficient and stable perovskite solar cells. *Organic Electronics* **2023**, *112*, 106689.
(S3) Golshani, Z.; Arjmand, F.; Maghsoudi, S.; Hosseini, S. M. A. Fe2O3–NiO doped carbon counter electrode for high-performance and long-term stable photovoltaic perovskite solar cells. *Journal of Materials Research and Technology* **2023**, *23*, 2612–2625.
(S4) Yang, X.; Qi, Y.; Wei, P.; Hu, Q.; Cheng, J.; Xie, Y. Enhanced efficiency and stability of carbon-based CsPbI2Br perovskite solar cells by introducing metal organic framework-derived Fe3O4@NC interfacial layer. *J. Power Sources* **2023**, *566*, 232927.
(S5) Huo, X.; Wang, K.; Liu, W.; Sun, W.; Yin, R.; Sun, Y.; Gao, Y.; You, T.; Yin, P. Synchronous Modulation of Energy Level Gradient and Defects for High-Efficiency HTL-Free Carbon-Based All-Inorganic Perovskite Solar Cells. *Small Methods* **2023**, *7* (7), 2300192.
(S6) Xiang, W.; Gu, X.; Khawaja, K.; Yuan, M.; Picart, C.; Li, L.; Yan, F. Low-dimensional carbon materials decorated FAPbI3 for carbon-based perovskite solar cells. *Carbon* **2025**, *235*, 120034.
(S7) Subramani, S.; Rajamanickam, G.; Perumalsamy, R. Fabrication of Affordable, Efficient, and Sustainable Carbon Electrode-based HTL-free Perovskite Solar Cells Using Azole Salts as Additive Material. *ACS Applied Energy Materials* **2025**, *8* (2), 1020–1030.
(S8) Fu, Y.; Shao, W.; Deng, Z.; Wu, W. Enabling high-efficiency ambient-air printable carbon-based large-area perovskite solar cells via effective anionic passivation. *Chemical Engineering Journal* **2025**, *503*, 158282..
(S9) Wang, J.; Gao, X.; Zhuansun, Y.; Zhu, D.; Liu, J.; Tang, L.; Wei, Q. Buried interface passivation with bis(3-aminopyrid-2-yl) sulfide for carbon-based perovskite solar cells. *Journal of Materials Chemistry C* **2025**, *13* (8), 3996–4005, 10.1039/D4TC04635H.
(S10) Zhang, B.; Zhao, Z.; Yu, F.; Chen, D.; Cheng, F.; Bala, H.; Zhang, Z. Enhanced efficiency and stability of inorganic CsPbBr3 perovskite solar cells based on carbon counter electrode by applying PbTiO3-coated TiO2 nanorod films as scaffold layers. *Materials Research Bulletin* **2024**, *175*, 112752.
(S11) Chen, Z.; Gui, L.; Wang, H.; Lu, X.; Wu, C.; Yang, X.; Li, Y.; Zhao, L.; Wang, S. Bifunctional π conjugated g-C3N4 for enhancing the efficiency and stability of carbon-based perovskite solar cells. *Separation and Purification Technology* **2025**, *362*, 131797.
(S12) Guo, D. e.; Ma, J.; Peng, H.; Yu, X.; Xue, J.; Xie, H.; Huang, H.; Kong, D.; Zhou, C. Breaking down the confinement effect on perovskite growth to fabricate efficient, carbon electrode-based mesoscopic perovskite solar cells via low-temperature and all-air procedures. *Journal of Materials Chemistry C* **2025**, 10.1039/D4TC04780J.
(S13) Riaz, S.; Liu, M.; Zhong, Z.; Mi, H.; Zheng, W.; Xiao, Y.; Qi, Y.; Qureshi, M. S.; Umar, S.; Xie, Y. Enhancing efficiency and stability in carbon-based perovskite solar cells through dual-interface modification. *Journal of Power Sources* **2025**, *630*, 236133.
(S14) Da, S.-J.; Liu, W.-W.; Li, C.-X.; Lei, Y.-X.; Ran, F. Regulation of Interface Schottky Barrier and Photoelectric Properties in Carbon-Based HTL-Free Perovskite Solar Cells. *Small* **2025**, *21* (5), 2408923.